Unraveling the Effect of Defects, Domain Size, and Chemical Doping on Photophysics and Charge Transport in Covalent Organic Frameworks

Raja Ghosh[*,†] and Francesco Paesani[*,†,‡,¶]

†*Department of Chemistry and Biochemistry, University of California San Diego, La Jolla, California 92093, United States*

‡*Materials Science and Engineering, University of California San Diego, La Jolla, California 92093, United States*

¶*San Diego Supercomputer Center, University of California San Diego, La Jolla, California 92093, United States*

E-mail: raghosh@ucsd.edu; fpaesani@ucsd.edu

Abstract

Understanding the underlying physical mechanisms that govern charge transport in two dimensional (2D) covalent organic frameworks (COFs) will facilitate the development of novel COF-based devices for optoelectronic and thermoelectric applications. In this context, the low-energy mid-infrared absorption contains valuable information about the structure-property relationships and the extent of intra- and inter-framework "hole" polaron delocalization in doped and undoped polymeric materials. In this study, we provide a quantitative characterization of the intricate interplay between electronic defects, domain sizes, pore volumes, chemical dopants, and three dimensional anisotropic charge migration in 2D COFs. We compare our simulations with recent experiments on doped COF films and establish the correlations between polaron coherence, conductivity, and transport signatures. By obtaining the first quantitative agreement with the measured absorption spectra of iodine doped (aza)triangulene-based COF, we highlight the fundamental differences between the underlying microstructure, spectral signatures, and transport physics of polymers and COFs. Our findings provide conclusive evidence of why doped COFs exhibit lower conductivity compared to doped polythiophenes. Finally, we propose new research directions to address existing limitations and improve charge transport in COFs for applications in functional molecular electronic devices.

TOC Figure

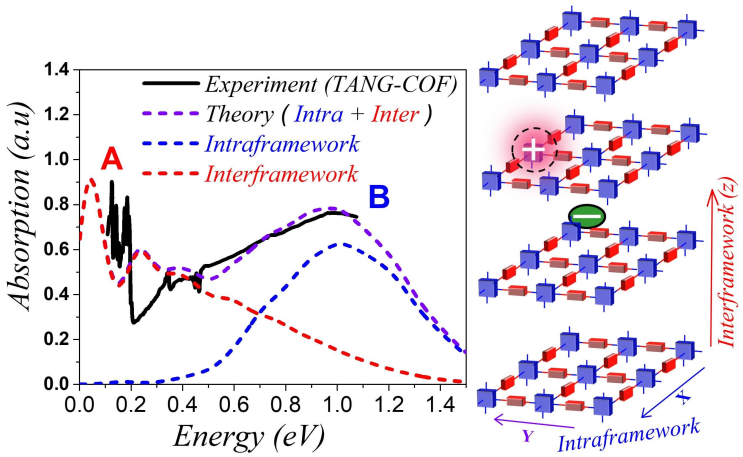

Introduction

COFs represent an emerging class of porous organic materials that offer a range of unique advantages compared to traditional polymers, such as morphological precision, high porosity, chemical stability, and positional control of diverse functional building blocks.[1–21] They form covalently linked two-dimensional (2D) polymeric π-sheets in the x-y plane where through-bond charge transport happens via coherent tunneling, while through-space charge hopping in the z direction occurs via significant wavefunction overlap between the π-stacked molecular columns.[22–24] This three-dimensional (3D) structural ordering enables inter- and intra-framework electronic interactions that facilitate efficient pathways for electron and polaron transport, thus making COFs promising materials for organic electronics. In this context, several key factors such as intra-framework molecular structure, inter-framework packing arrangement, and long- and short-range order within the COF domains can significantly influence hole movement both along the 2D planar sheets and through the 1D columns, thus affecting charge carrier mobility, conductivity, and overall device performance.

Polaron delocalization in organic materials can be identified from and directly correlated to the low-energy spectral lineshape and position of the mid-infrared absorption spectrum. Formation of "hole" polarons in organic materials, optically (e.g., by photoinduction), electrochemically (e.g., by applying gate voltage) or in the presence of chemical dopants, gives rise to significant absorption in the mid-IR energy range, which is characterized by a low-energy peak A (0.05-0.2 eV), dressed with intramolecular vibrations (IRAVs), and a much broader higher energy peak B (> 0.25 eV).[25–31] The A peak is labelled as DP_1 (delocalized polaron)[26,32] or CT (charge transfer),[25,33,34] while the B peak is commonly referred to as P1[25,26,30] in the conventional polaron model. In conjugated polymers, such as P3HT, a red-shift of peak B(P1) is either related to increased polaron delocalization lengths[26–28,30,35] or the formation of spin-less non-radical bipolarons.[36] However, unlike conjugated polymers, ESR signals from sp^2 carbon conjugated COFs confirmed the absence of bipolaron formation.[11] Later, theoretical simulations demonstrated that at high dopant concentrations, p-dopants

form a charge-transfer complex with the COF structures, leading to localized electronic states and spin-polarized COFs, thus ruling out the possibility of bipolarons.[37] The characteristic low energy-peak A and the blue-shifted broad peak B is evident in the mid-IR absorption spectra of iodine doped (aza)triangulene-based COF (TANG-COF) which exhibit high in- and out-of-plane conductivity.[31] COFs exhibit a dramatic but reversible increase in conductivity upon exposure to iodine.[11,38–40] Vapor doping tetrathiafulvalene-based COFs with iodine results in a significantly larger increase in conductivity compared to solution doping with TCNQ.[41–43] Finally, it was shown that the F_4TCNQ-doped 2D imine-linked COF, based on the electron-rich Wurster-motif (WBDT), yields higher conductivities compared to when doped with iodine.[44] Interestingly, unlike iodine, higher conductivities due to F_4TCNQ were not only stable and irreversible but also retained the crystallinity of the COF structure.

In the absence of chemical dopants, photoinduced "hole" polarons were generated in oriented benzodithiophene COF thin films.[45] The hole mobility was measured both in the COF plane and through the 1D-columns, leading to the conclusion that charge mobility depends on the thickness of the COF films, with thicker films being associated with lower hole mobility. This low mobility in thicker films can be attributed to the presence of electronic defects, as well as to disorder at grain boundaries or in the interlayer stacking arrangement.[46–50] The size of the COF crystalline domains can also impact charge transport. In particular, defects arising from non-crystalline regions can trap the polarons, resulting in localization and subsequently yielding lower values of hole mobility and conductivity. The effects of domain size,[28,51] electronic defects,[52–54] crystallinity,[55,56] molecular weight,[33] side chain engineering,[57] and chemical dopants[30,35,58,59] have been previously discussed in the context of conjugated polymers. In all these cases, mid-IR polaron signatures have provided fundamental insights into local structure-property relationships and have successfully established key correlations between polaron coherence and hole mobility.[28]

It is therefore particularly relevant to potential optoelectronic applications of COFs to understand how incorporating anions within frameworks having different linkers and pore

volumes impact the mid-IR spectra and polaron coherence lengths. It is also equally important to investigate the effect of domain impurities, defects, and stacking dislocations on the spectral signatures. To this purpose, we introduce a 3D Holstein-style model for polarons[29] which treats static defects, electronic coupling, and lattice vibrations on equal footing to model tetragonal COF structures. Importantly, our model also identifies spectral signatures from which the generally anisotropic polaron coherence lengths, both along the x and y directions within the 2D COF plane and through z direction along the 1D columns, can be readily determined. We study the impact of electronic defects on charge transport in 2D COF structures and show how mid-IR spectral signatures can be effectively used to distinguish between large and small crystalline COF domains, crystalline and amorphous frameworks, and track the relative position of the dopant counteranions in the vicinity of the frameworks. By comparing our simulated spectra with the measured absorption spectra of doped TANG-COF,[31] doped WBDT COF,[44] and doped TTF-COF films,[41] we not only establish the similarities and differences between the measurements but also emphasize the need to perform specific experiments which can further our understanding of charge transport processes in COFs. Furthermore, by differentiating the microstructure and spectral signatures of doped polymers and doped COF films, our analysis provides direct evidence of why high charge mobility in COFs has only been observed over short distances, and long-range mobility measurements have so far yielded significantly lower values. Finally, we conclude by laying down design strategies which may be helpful for synthesizing better COF-based devices for potential use in optoelectronic applications.

Theoretical Model

Our theoretical model is based on a coarse-grained Holstein-style Hamiltonian in which electronic coupling, vibronic coupling involving the prominent quinoidal-aromatic stretching mode, and static defects (e.g., torsional and structural defects, and lattice imperfection)

are treated on equal footing to obtain the hole wavefunctions and energies, without making the Born-Oppenheimer (BO) approximation.[29,52–54,60] The key aspect of our approach is the nonadiabatic treatment of the vibronic coupling involving the symmetric mode: both the nuclear kinetic and potential energies are treated fully quantum mechanically. The two dimensional Holstein model has already been successful in rationalizing various experiments carried out on semiconducting polymers.[27,30,35,57–59,61] Using our model we can not only obtain quantitative agreement with experiments but also extract detailed information about the polaron coherence lengths, i.e, how far the hole delocalizes along the x and y directions in the 2D COF plane and through the columns (z directions). The full theoretical framework, including a description of the multiparticle basis set, expressions for the IR absorption spectrum, disorder, coherence functions, Coulomb binding, and the fundamental nature and origin of the IR peaks are discussed in detail in the Supporting Information. All simulations are carried out for 3D frameworks with up to 5×5×4 (i.e., 84) coupled monomeric units, which are sufficient to achieve complete spectral convergence and remove finite size effects.

Results and Discussion

Effect of Domain Size and Electronic Defects

Perfect covalent connectivity and large crystalline domains are essential for long-range coherent transport of charges. Reversible formation of covalent bonds is one of the most widely used techniques to achieve higher crystallinity in COFs.[62] Pyrene based building blocks having synchronized offset-stacking were used to design crystalline COFs with domain sizes as large as half a micrometer.[63] However, achieving large crystalline domains can be experimentally challenging as defects arising due to bond breakage, stacking faults, steric repulsions, and pore collapse can result in amorphous frameworks and smaller domains on the order of a few hundred nanometers.[62] We begin our analysis by comparing the IR absorption spectra and the 2D coherence function of the holes that are generated either optically (photoinduced

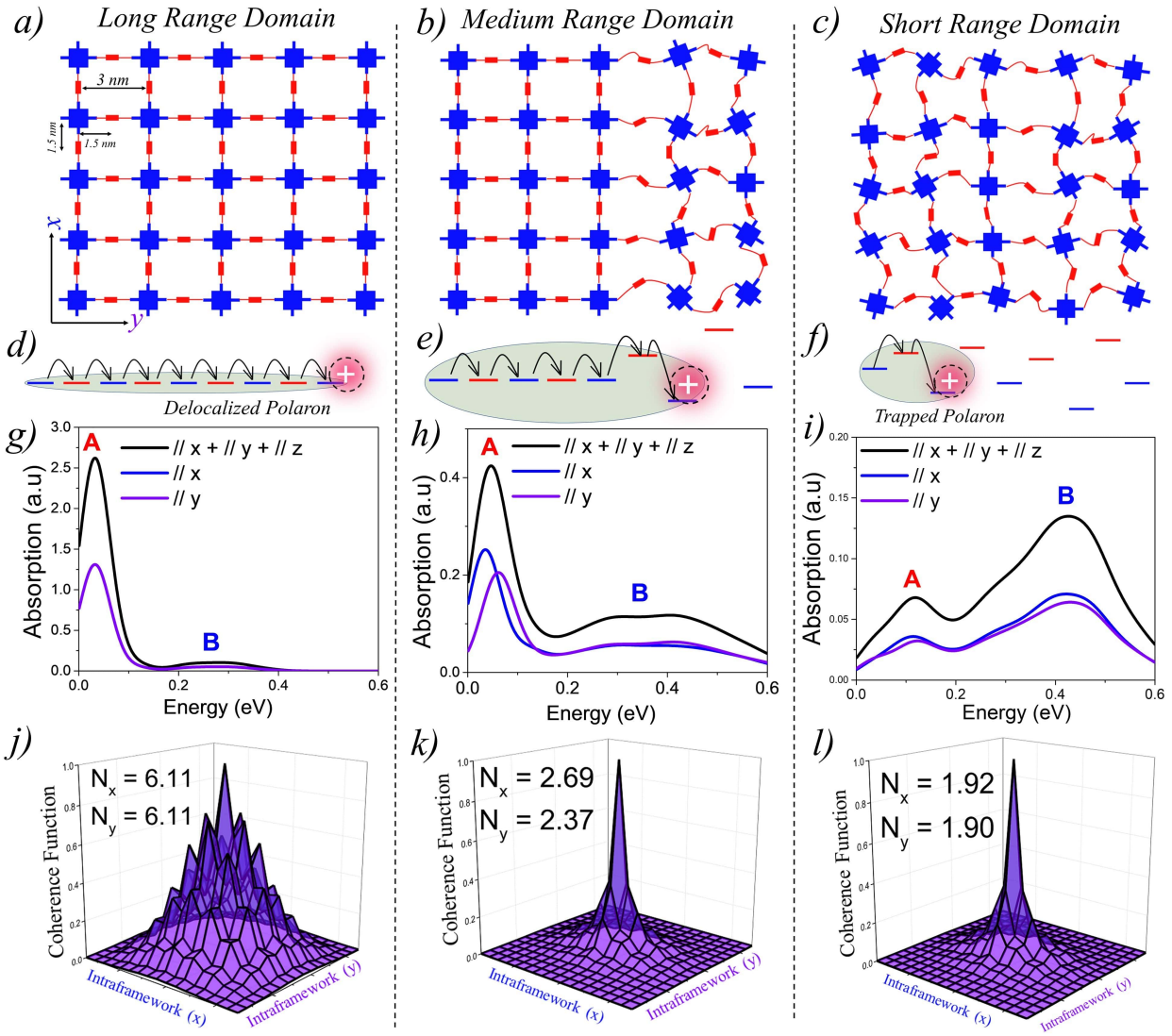

Figure 1: (a-c) Schematic representations showing long-range, medium-range and short-range 9×9 (i.e., 9 and 5 units along the x and y directions alternatively) COF domains with a pore size of 3 nm and a separation of 1.5 nm between each repeat unit. (d-f) Representation of site energy fluctuations due to static disorder. (g-i) Hole mid-IR absorption spectrum for a 9×9 tetragonal COF lattice having a disorder width (σ) of 0.3 eV. An average over 5000 disorder configurations was performed for each spectrum to guarantee convergence. The associated coherence functions are shown in (j-l). All the parameters of the Hamiltonian defined in Eq. S1 are given in the Supporting Information.

absoprtion spectroscopy) or electrically (charge modulation spectroscopy). We consider a 2D tetragonal COF structure having long-range, medium-range and short-range crystalline domains as illustrated in Fig. 1(a-c). In all the three cases, the pore size is taken to be 3 nm and adjacent units are 1.5 nm apart. Majority of COF structures have a a pore size between

2 to 4 nm. For simplicity, and in order to emphasize the impact of electronic coupling, we assume identical charge-transfer (CT) integrals and set them to 0.20 eV along both the x ($t_{intra-x}$) and y ($t_{intra-y}$) directions, which is a good approximation for tetragonal COF structures.[37] However, $t_{intra-x}$ and $t_{intra-y}$ can vary depending on functionalization and/or the presence of out-of-plane defects, either along the x or y directions in the 2D plane (these effects will be taken into consideration in the next sections).[64] All the other parameters of the Hamiltonian are given in the Supporting Information. Fig. 1g shows the absorption spectra and 2D coherence function for an ideal defect free 9×9 lattice, i.e, a lattice with long-range π-conjugated building blocks and devoid of any defects. The total absorption spectrum is shown in black and the x and y components are shown in blue and violet, respectively. In the absence of defects, the hole can efficiently migrate over the entire 2D plane (both along x and y) resulting in a red-shifted absorption peak revealing the presence of "hole" polarons in the mid-IR, which are responsible for charge carrier mobility. The polaron cloud is isotropically delocalized over roughly $N_x = 6.11$ ($N_y = 6.11$) units along the x (y) directions in the 2D plane. In the absence of defects, the IR absorption and coherence lengths along x and y axes are exactly the same due to identical values of electronic coupling. The situation is profoundly different in the presence of electronic defects. As defects slowly creep into the framework (Fig. 1b), disorder- induced polaron-trapping affects hole transport in medium-range domains. This results in a reduction of the width of the coherence function, attenuation of the spectral intensity (both along the x and y directions), and the formation of two distinct bands A and B. The drop in the calculated band oscillator strength in medium-range domains tracks a similar drop in the polaron delocalization lengths along x (N_x=2.69) and y (N_y=2.37), respectively. As shown schematically in Fig.1(e-f), introducing disorder leads to energetically isolated monomeric units resulting in trapped polarons which can no longer absorb IR photons. In contrast to neutral excitons, where the oscillator strength in the UV-vis region gets redistributed,[65–68] the oscillator strength in the case of polarons is not conserved, thus leading to spectral attenuation.[29] Apart from the loss in spectral intensity,

two extremely important signatures of defects involve the gradual change in the ratio of the spectral intensities of peaks A and B and the broadening of peak B. The evolution of the spectral signatures with increasing defect density is clearly evident in short-range domains, where the A/B peak ratio is less than one, and is accompanied by a blue-shifted broad peak B. The polaron delocalization lengths along x and y further diminish to 1.92 and 1.90 repeat units, respectively. For excitons, which absorb in the UV-vis region,[67–69] a red shift of the UV-vis spectrum generally indicates delocalized excitations. For polarons, a red shift (blue shift) of peak B and a larger (smaller) A/B peak ratio implies larger (smaller) polaron delocalization lengths. Therefore, polaron absorption from different domain sizes will be different unlike in the case of excitons for which it has recently been shown that the absorption remains the same while the emission changes drastically.[15] Peak B in the IR spectrum in any direction (x, y ,z) is an electronic transition from the ground state of the polaron to the next higher electronic state in the same direction. We emphasize that peak A is an electronic transition and is distinct from the superimposed narrow resonances also observed in the the experimental measurements which are instead due to IRAV modes. The calculated spectral intensity of peak A relative to B changes as a function of polaron delocalization in agreement with the measurements as shown in Figs.6a and 5a. The shape of peak A and the decrease of the A/B peak ratio with increasing disorder in any direction can be qualitatively understood in terms of an Herzberg-Teller coupling mechanism.[29,53,54] The fundamental nature and origin of both peaks, along with a detailed mathematical formulation, are discussed in Refs.[29,53,54] and summarized in the Supporting Information.

Engineering long-range crystalline COFs is a challenging task, and, within each crystalline domain, crystallinity is usually measured by the degree of chemical defects, torsional disorder, and structural faults. In Fig. 2c, we characterize the impact of increasing disorder on the total absorption spectrum for the same 9×9 2D tetragonal COF lattice. As the disorder width (σ) is gradually increased, i.e, as we transition from a perfectly crystalline framework to an amorphous framework, the spectral signatures follow the same trend. Increasing σ results in

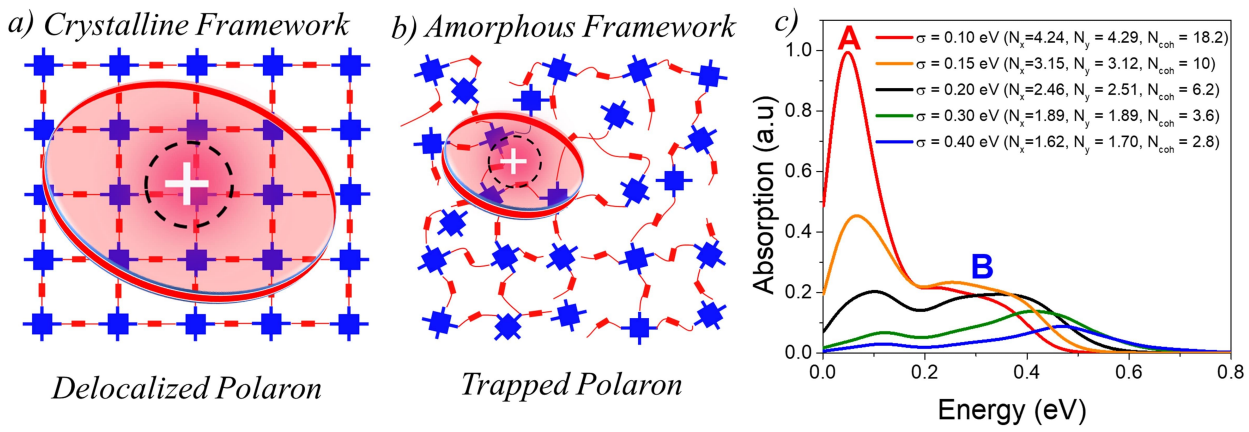

Figure 2: (a-b) Schematic representations of crystalline and amorphous frameworks having delocalized and localized polaron cloud, respectively. (c) Hole absorption spectrum in the mid-IR energy range for a 9×9 tetragonal COF framework having a pore size of 3 nm for different values of σ. An average over 5000 disorder configurations was performed for each spectrum to guarantee convergence. All the parameters defining the Hamiltonian in Eq. S1 are given in the Supporting Information.

a dramatic loss of oscillator strength, blue shift and broadening of peak B, reduction of the coherence lengths, and a decreasing A/B peak ratio. The total polaron coherence numbers N_{coh} (approximately equal to the product of N_x and N_y) as a function of σ are reported in the inset of Fig. 2c.

Importance of Polarized Measurements on Oriented COF films

In the previous section, we have analyzed the IR absorption spectra of model COF systems across the 2D xy plane where the electronic interactions are essentially "through-bond". The model can be further extended in the third dimension (z) to include "through-space" π-π interactions between the 2D polymeric layers in the 3D frameworks. We focus on the impact of electronic defects on the IR spectrum of a 5×5×4 framework hosting a single hole and having a pore size of 3 nm with each repeat unit in the COF plane separated by a distance of 1.5 nm. The π stacking distance between the 2D sheets is taken to be 0.4 nm. In our simulations, we consider four different scenarios as illustrated in Fig.3(a-d) and use realistic coupling parameters for prototypical COF structures calculated in Ref. 70.

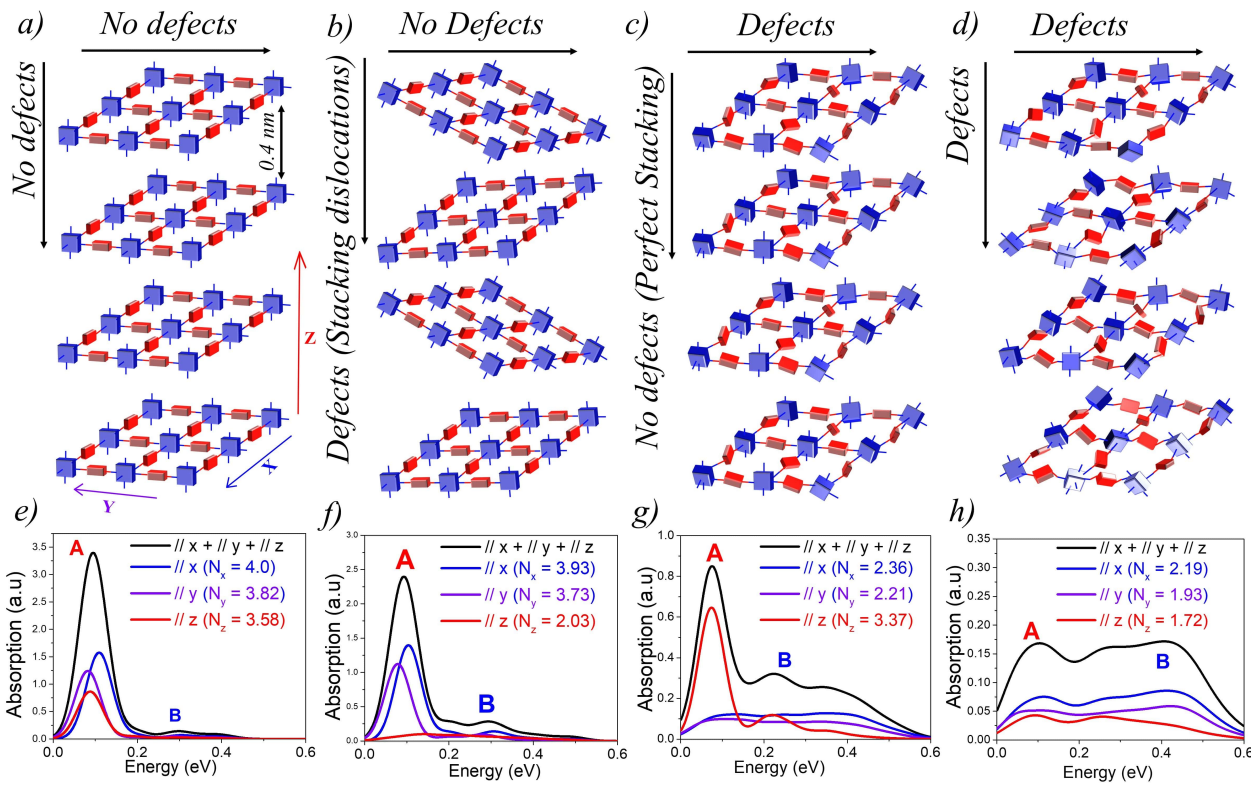

Figure 3: Schematic representations of 5×5×4 frameworks with: (a) perfect 3D order, (b) inter-framework/columnar defects; (c) intra-framework/in-plane defects, and (d) both inter- and intra-framework defects. The associated hole absorption spectrua for all the four scenarios are shown in (e-h). All the parameters of the Hamiltonian defined in eq. S1 are given in the Supporting Information.

In the first scenario, we consider an ideal defect-free 3D framework (Fig.3a, Fig.S3a), and assume slightly different values of $t_{intra-x}$ (0.25 eV) and $t_{intra-y}$ (0.22 eV) in order to distinguish between the x and y components of the IR spectrum. The total absorption is shown in black while the x, y, and z components are shown in blue, violet, and red, respectively. The polaron wavefunction is approximately spread over $N_x = 4.0$, $N_y = 3.82$, and $N_z = 3.58$ units along the x, y and z directions, respectively. In the second scenario, we consider inter-framework columnar disorder(Fig.3b, Fig.S3b), with perfect crystalline connectivity and planar arrangement of the monomers within the 2D sheets, and disorder only between the molecular stacks (Fig. 3b). As shown in Fig. 3f, the gradual increase in the inter-framework disorder (σ) results in the selective attenuation of the spectral intensity and

drop in coherence length only along the z component (red) compared to the disorder-free spectrum (Fig. 3e). While the polaron delocalization lengths along x ($N_x = 3.93$) and y ($N_y = 3.73$) remain relatively unchanged, the polaron delocalization length along z drops to $N_z = 2.03$ units. In the third scenario, disorder only exists in the 2D sheets and the perfectly aligned stacks are essentially defect-free(Fig.3c, Fig.S3c). As shown in Fig. 3g, the disorder selectively attenuates the x and y components in the 2D plane, while leaving the z component relatively unchanged. The coherence lengths follow the same trend as shown in the inset of Fig. 3g. Finally, in the fourth and most realistic scenario, we consider both intra- and inter-framework disorder(Fig.3d, Fig.S3d) which lead to spectral attenuation of all the components. The overall polaron cloud further contracts and is now found to approximately spread over $N_x = 2.19$, $N_y = 1.93$, and $N_z = 1.78$ units along the x, y, and z directions, respectively. Increasing disorder along any axis results in the shrinking of the coherence function, attenuation of the spectral intensity, blue shift and broadening of peak B, and decreasing A/B peak ratio along the same axis. Therefore, the relative position of the peak B maximum and the ratio of the A/B peak directly correlates with polaron coherence. This implies that a small (large) A/B peak ratio along any axis (x, y, and z) can be readily interpreted as a measure of polaron delocalization lengths along the same axis.

Hence, polarized mid-IR measurements on oriented COF samples, although experimentally challenging, can be a breakthrough in advancing the fundamental understanding of charge transport, both within the 2D sheets (xy plane) and through the columns (z direction), since it allows for exploiting the in- and out-of-plane band oscillator strengths and the polaron coherence lengths. Specifically, the intra- and inter-framework polarized components of the mid-IR spectrum contain complementary information about hole localization, which can be further used to quantify the degree of disorder and the local microstructure within individual COF domains.

Effect of Chemical Dopants

The presence of electron withdrawing dopants like iodine, which has been commonly used to dope several COF structures, leads to the creation of "hole" polarons, resulting in an increase in hole mobility and conductivity. These polarons are generally referred to as "bound" polarons since they are Coulombically bound to the dopant counter-anions and exhibit reduced coherence lengths compared to unbound or "free" holes, which are generated either optically (photoinduced) or electrically (gate voltage). In the case of doped conjugated polymers, for which F_4TCNQ has been extensively used as p-dopant, it has been shown both experimentally[55] and theoretically,[53,54] that the counter-anions preferentially reside either in the amorphous regions close to the grain boundaries or in the lamellar regions, but do not intercalate between the crystalline π-stacks.[55] The preferable location of the counter-anions in the polymer matrix not only affects the polaron coherence lengths but also impacts the mid-IR spectral signatures. In the case of doped COFs, the iodine counter-anions can be easily incorporated inside the pores, with COFs having larger porous volumes and surface area favoring maximum intake. It was found that the TTF-based 3D COF,[43] which is characterized by larger pore volumes compared to its 2D counterpart, displays much higher conductivity upon iodine doping.[41] Before comparing our results with the available experimental data, we demonstrate that the position of the dopant anions, either within the porous channels or in the amorphous domains, can anisotropically impact the intra- (x, y) and inter-framework (z) components of the mid-IR absorption spectrum and the polaron coherence functions. More importantly, these spectral signatures can be efficiently used to identify the possible location of the counter-anions in the vicinity of the COF structures.

In order to appreciate the impact of dopant anions on the mid-IR absorption spectrum, we monitor the evolution of the intra- and inter-framework components of the absorption spectrum and the coherence lengths by gradually changing the position of the dopant anion relative to the framework. As shown in Fig. 4, positions 1-6 correlates to the anion located: at an infinte distance away (i.e no anion), at a distance of 0.8 nm and 0.4 nm from the

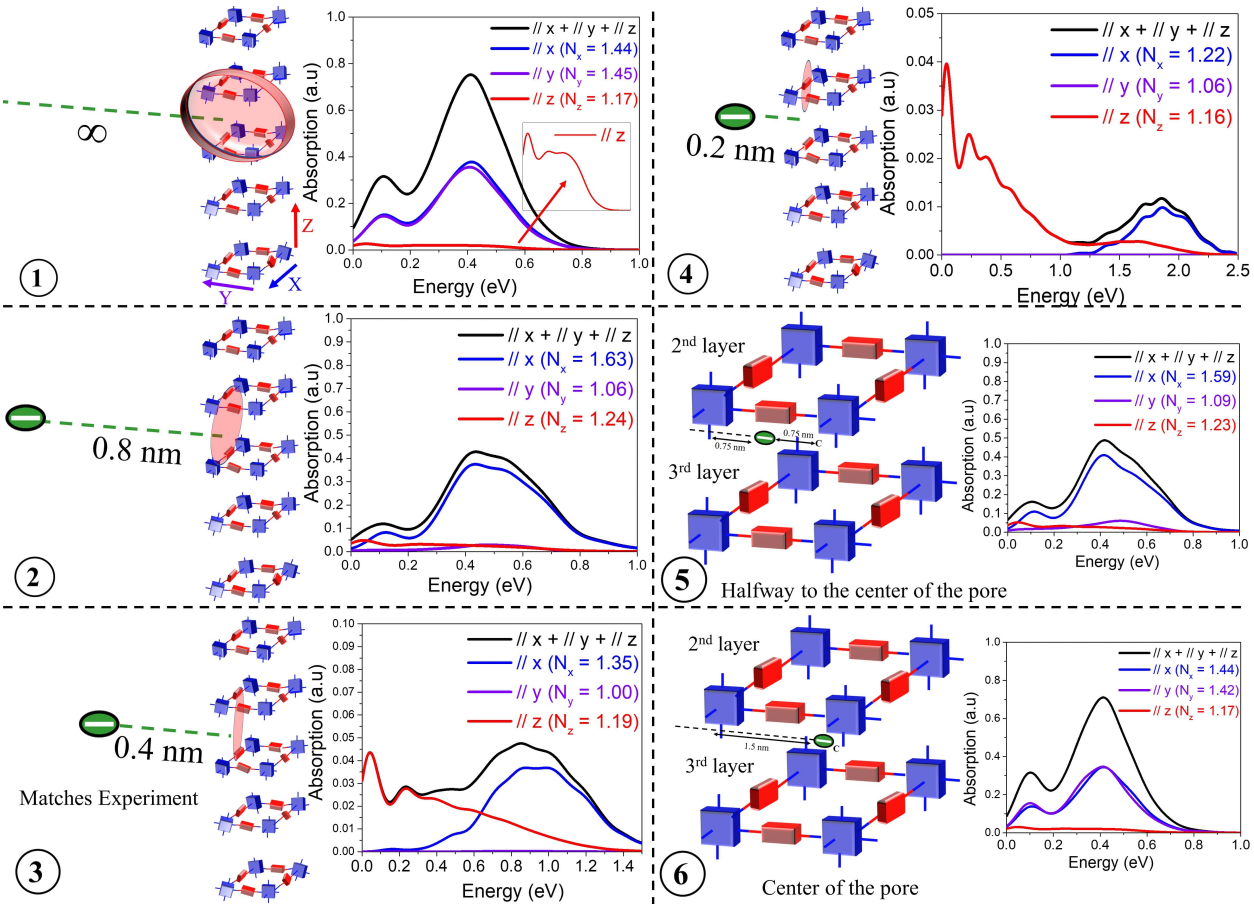

Figure 4: Calculated IR spectrum of a disordered 3×3×5 COF framework for various positions of the dopant counter-anion relative to the COF structure. All the parameters of the Hamiltonian defined in Eq. S1 are given in the Supporting Information.

framework, very close to the backbone (0.2 nm), halfway from the center of the pore, and in the center of the pore. Placing the anions at a distance of 0.4 and 0.8 nm from the framework signifies the presence of the dopants in the amorphous regions between two crystalline domains and its relevance will be discussed in the next section. In the absence of chemical dopants, i.e, when the anion is at an infinite distance away, the mid-IR absorption spectrum and the polaron coherence function is solely determnined by the localizing effects of disorder and the magnitude of the CT integrals. As the anion approaches the framework, Coulomb binding can also localize the hole, in addition to disorder induced traps. Finally, when the anion resides in very close proximity to the hole, significant Coulomb binding is now the predominant factor in hole localization compared to disorder induced effects. In this regime

of strong Coulomb binding, slight variations in the coherence wavefunction can correlate to dramatic changes in the IR spectrum.

Fig. 4 shows the disorder-averaged IR spectra for a 3×3×5 tetragonal COF framework for each of the six anion positions calculated using physically realistic electronic couplings from Ref. 37. The tetragonal COF framework has a pore size of 3 nm with each repeat unit along the x and y axes separated by a distance of 1.5 nm. The π-stacking distance between the 2D layers is taken to be 0.4 nm. In the absence of dopants, the polaron wavefunction is approximately spread over an equal number of units along x (N_x=1.44) and y (N_y=1.45) due to identical values of electronic couplings ($t_{intra-x,y} = 0.14eV$) and disorder width ($\sigma = 0.25eV$). This is reflected in the IR absorption where the x (blue) and y (violet) components show similar spectral signatures, while the z (red) component is substantially diminished since the through-space inter-framework hopping integral is significantly smaller ($t_{intra-z} = 0.025eV$) compared to the through-bond intra-framework integral, in agreement with DFT calculations.[37] The polaron delocalization length along z is (N_y=1.17). The A/B peak ratio is tiny because, within the COF plane, the number of units along the x and y axes is limited to a maximum of three. A larger framework (e.g., 5×5×5), would enable greater polaron delocalization and result in a higher A/B ratio as demonstrated in the previous sections. However, as shown later, a 3×3×5 framework is sufficient for direct comparisons with the experimental data. In position 2, as the anion is brought closer to the framework (0.8 nm), strong Coulomb binding attracts the hole towards itself, and the hole is able to delocalize only over the units closer to the anion (red shaded region) along the x (N_x=1.63) and z (N_x=1.24) axes, with negligible hole movement along y (N_x=1.06). As a result of localization along y, while the x and z components remain relatively unchanged, the spectral intensity along the y component greatly diminishes and exhibits a blue shift. Bringing the anion even closer (0.4 nm) to the framework results in very strong Coulomb binding, which greatly localizes the hole, restricting its movement entirely along the x and z axes. Even along the x and z axes, the polaron coherence decreases to N_x=1.35 and N_y=1.19, respectively, due to the

closer proximity of the anion relative to the framework. This strong effect of localization can be understood from the analysis of the IR spectrum showiing that the y component completely vanishes, which is accompanied by a significant drop in spectral intensity and blue shift of the x component. The spectral intensities along the x and z components are similar despite $t_{intra-x}$ being significantly larger compared to $t_{inter-z}$. In position 4, where the anion is right next to the backbone (0.2 nm), the x component is further attenuated and considerably blue shifted compared to the z component. The associated polaron coherence numbers for position 4 are reported in the inset of Fig. 4. In position 5, as the anion is moved inside the framework and positioned halfway from the center of the pore, i.e, placed at a distance of 0.75 nm from the x axis and 0.75 nm from the center of the pore, the strength of the Coulomb binding decreases. With decreased Coulomb attraction and increased polaron delocalization lengths, the x component starts to red-shift and grows in intensity while the y component still remains insignificant. Finally, when the anion is placed at the center of the pore, and all the units along the x and y axes are equidistant from the anion and experience equal strengths of Coulomb binding, the spectral signatures and coherence lengths are similar to position 1. It should be noted that the polaron delocalization lengths along z and the inter-framework component of the absorption spectrum remain approximately similar across all the anion positions due to smaller values of electronic coupling. If higher values were used, the evolution of the interframework component (z) would show the same trend as observed along x and y. This analysis systematically demonstrates how the inter- and intra-framework components in the IR spectrum anisotropically respond to the position of the dopant counter-anion relative to the framework. For our analysis, we have laterally displaced the anion (from infinity to center of the pore) perpendicular to the x axis. If we had instead moved the anion parallel to the x axis, the x and y components of the IR spectrum will interchange keeping the total absorption unchanged. The total absorption spectrum (black) in position 4 is in qualitative agreement with the measured absorption spectrum of iodine doped TANG-COF.[31] This comparison indicates that the experimental spectrum

corresponds to the configuration where the closer proximity of the anion relative to the framework substantially localizes the polaron wavefunction to only 1.35, 1.00, and 1.19 units along the x, y, and z directions. It should be noted that, had we used a larger framework, the polaron coherence lengths and spectral signatures would remain unchanged due to very strong localization effects. Therefore, in all comparisons to experiments presented in the following sections, we will resort to a 3×3×5 framework hosting a single hole and having one dopant counteranion.

Comparison to Experiment

Two-dimensional Poly(azatriangulene) COF

Based on the approach described in the previous sections, we proceed to compare our simulations with the recently measured mid to near IR (unpolarized) absorption spectra of doped COF films. In order to understand why doped COFs have so far shown lower conductivity compared to doped polythiophenes, it is important to compare the mid-IR spectral signatures of iodine doped regioregular (RR) and regiorandom (RRa) P3HT[26] with iodine doped TANG-COF.[31] In the case of highly amorphous RRa-P3HT films, the polarons are localized on isolated P3HT chains due to random orientation of the side groups which hinder aggregate formation. Moreover, Coulomb binding with the anions that reside in the amorphous domains close to the isolated polymer backbones can also localize the hole. The position of peak B is around 0.5 eV and the A/B peak ratio is approximately 0.6. In marked contrast, for the highly ordered and aggregated RR-P3HT, which enables greater polaron delocalization, as expected, there is a red shift of peak B which is accompanied by a dramatic increase in the A/B peak ratio (≈ 1.6). The enhanced polaron delocalization in RR-P3HT is attributed to aggregation, greater crystallinity, and weak Coulomb binding, since the dopant anions in RR-P3HT have been shown to preferentially reside either in the lamellar region or in the amorphous domains of the polymer matrix but do not intercalate between the crystalline

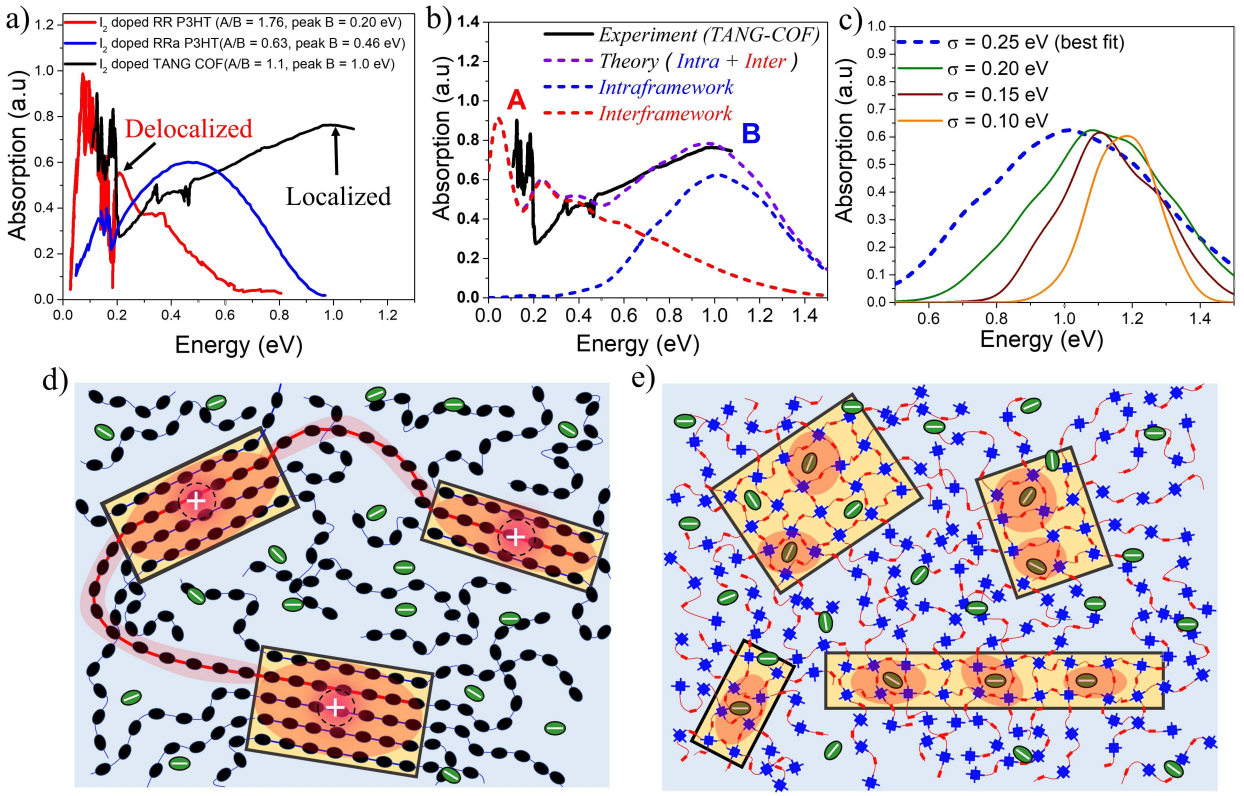

Figure 5: (a) Comparing the mid-IR absorption spectrum of iodine doped P3HT(replotted froom Ref. 26) and iodine doped TANG-COF(replotted froom Ref. 31). (b) Comparison of the simulated IR spectrum (dashed) to the measured IR spectrum of iodine doped TANG-COF.[31] (c) Intraframework component of the infrared absorption as a function of σ.(d) Sketch showing long tie-chains (red shaded regions) interconnecting crystalline domains resulting in higher mobility in high molecular weight conjugated polymers.(e) Sketch showing localized polaron wavefunctions (red shaded regions) within individual COF domains due to strong coulomb binding with iodine dopants that resides in the porous channels resulting in lower conductivity and disordered frameworks.

π-stacks.[55] In the IR spectra of iodine doped TANG-COF, the peak B is significantly blue-shifted and shows a maximum around 1 eV. Interestingly, unlike RRa-P3HT, the A/B peak ratio in TANG-COF is much greater and close to one. Finally, all the three experimental measurements display sharp anti-resonances (0.05 eV - 0.2 eV) due to IR active vibrations (IRAVs). We do not account for IRAVs in our theory, rather, we are more concerned with the overall spectral envelope, i.e peak A.

The simulated absorption spectrum for the TANG-COF is based on the Hamiltonian in Eq. S1 and is shown in Fig. 5b. In order to reproduce the experimental absorption

spectrum, we consider an anion located inside the pore of an oxidized 3×3×5 framework hosting a single hole. To quantitatively mimic the spectral details, in particular, the blue shifted nature of peak B, it is necessary to bring the anion closer to the framework. Since it is unphysical for the anion to be located exactly at one position, in order to obtain the best fit, the simulated spectrum has been averaged over several anion positions as detailed in the SI (Fig. S6). Our analysis shows that the dopant counteranions most propably reside at a distance of 0.3-0.45 nm from the framework. The parameters used to define the Hamiltonian have been explicitly justified in the SI which shows that the model is robust and our conclusions remain unchanged with slight variations in the parameters. Overall, the agreement with the experimental spectrum is very good, with the theoretical model capturing most of the salient features of the measured spectrum except the red-shifted peak A. As can be readily appreciated from the blue curve in the simulated spectrum (Fig. 5b), peak B entirely originates from the intra-framework component of the absorption spectrum. The greatly blue shifted absorption around 1 eV is a trademark signature of localized polarons. It is a clear indication that the dopant counteranions reside in very close proximity to the framework, thus affecting hole movement within the 2D-COF plane. This can be understood by considering that the iodine vapors readily diffuse into the pores of the frameworks and trap the polarons via strong Coulomb attraction.

In order to more thoroughly investigate the broad nature of the intra-framework component (peak B), in the following analysis we keep all the Hamiltonian parameters fixed and gradually change the disorder width (σ). The influence of disorder is very clearly demonstrated in Fig. 5c, which shows how the intra-framework absorption spectrum responds to increased σ. While it is necessary to bring the anions closer to the framework to correctly reproduce the position of the peak B maximum, an increased disorder width of 0.25 eV is needed to accurately reproduce the broadening. This shows that the presence of excessive anions in the pores most likely creates defects within the 2D COF planes thus resulting in unstable and reversible conductivity. Our results comply with recent DFT-based calcula-

tions which show that excessive doping result in localized electronic states and metal free magnetism.[37] While COFs can be good candidates for magnetism, it seems they may not be great for charge transport. Luckily, there is ample scope for improvement as demonstrated in Ref. 44 and will be discussed later.

As shown in Fig. 5b, peak A centered around 0.12-0.15 eV entirely originates from the inter-framework component (red curve) of the simulated absorption spectrum. Unlike conjugated polymers, COFs form a three-dimensional structural arrangement and through-space charge hopping happens along the molecular columns. However, it should be noted that in the absence of chemical dopants (free holes), the low energy peak A can also arise from (equal or unequal) contributions from both intra- and inter-framework components of the absorption spectra as shown in Fig.3(e-h). In these scenarios, we can expect to see an even higher A/B ratio similar to what has been previously observed in the case of electrochemically, chemically, and optically doped conjugated homopolymers and donor acceptor copolymers.[27,28,71] However, this claim needs to be verified and more experiments need to be conducted to understand the fundamental polaron photphysics, charge transport properties of COF structures and the nature of the two bands in the IR spectrum.

While it is true that an increase in polaron delocalization lengths is directly associated with an increase in hole mobility and conductivity, it is important to emphasize that polaron coherence occurs at the nanoscale and is constrained within individual crystalline domains, while mobility and bulk conductivity is a mesoscale phenomenon.[28,59,72,73] This is true since the movement of even the most coherent polaron in an ideal defect-free crystalline domain is ultimately restricted by the size of the domain and the domain boundary. It has recently been demonstrated that both polaron coherence and hole mobility increases only till a certain point with an increase in the molecular weight of 100% RR-P3HT. However, with further increase in the molecular weight (>12.6 kg mol^{-1}), while polaron coherence remains stagnant, mobility keeps on increasing.[28] The increase in hole mobility for high molecular weight RR-P3HT and copolymers has been attributed to the presence of long tie chains that

interconnects crystalline domains.[72–74] The schematic microstructure of the high molecular weight polymers in Fig. 5d shows the nature of charge transport between crystalline domains via tie chains, which results in higher mobility/conductivity while the dopants reside in the amorphous domains far away from the crystalline regions. In marked contrast, the blue-shifted nature of peak B in doped TANG-COF clearly suggests, that within individual COF domains, as shown in Fig. 5e, polaron delocalization is severely affected due to the formation of Coulomb induced trapped polarons that hampers conductivity and final device performance.

Therefore, low conductivity in iodine doped COF films compared to conjugated polymers can be associated with three most probable causes: 1) strong Coulomb binding with the dopant counteranions in the porous channels localizes the hole within individual COF domains, 2) excessive iodine doping may result in pore collapse, loss of crystallinity, and amorphous frameworks, and 3) unlike polymers, hole transport between COF domains has not been possible so far and to the best of our knowledge, no mechanism of inter-domain charge transport has come to light.

Wuster Benzodithiophene-Dialdehyde COF

A highly crystalline imine-linked COFs based on the electron-rich Wurster-motif and benzodithiophene dialdehyde (WBDT COF) was reported in Ref. 44. Doping WBDT COF with iodine and F_4TCNQ yield conductivities of 4.72×10^{-2} S m^{-1} and 3.67 S m^{-1}, respectively. However, F_4TCNQ doping not only shows higher, irreversible and stable conductivity but also retains the crystallinity of the framework.

The impact of doping by various dopants can be correlated to the changes in the mid to near IR spectral signatures. Despite WBDT-COF having a different structural arrangement compared to TANG-COF, the infrared spectrum of iodine doped WBDT COF shows that the position of the peak B maximum is centered at $\sim$1 eV (Fig. 6a). This demonstrates that, irrespective of topology, the iodine dopants indeed occupy the porous channels and localize

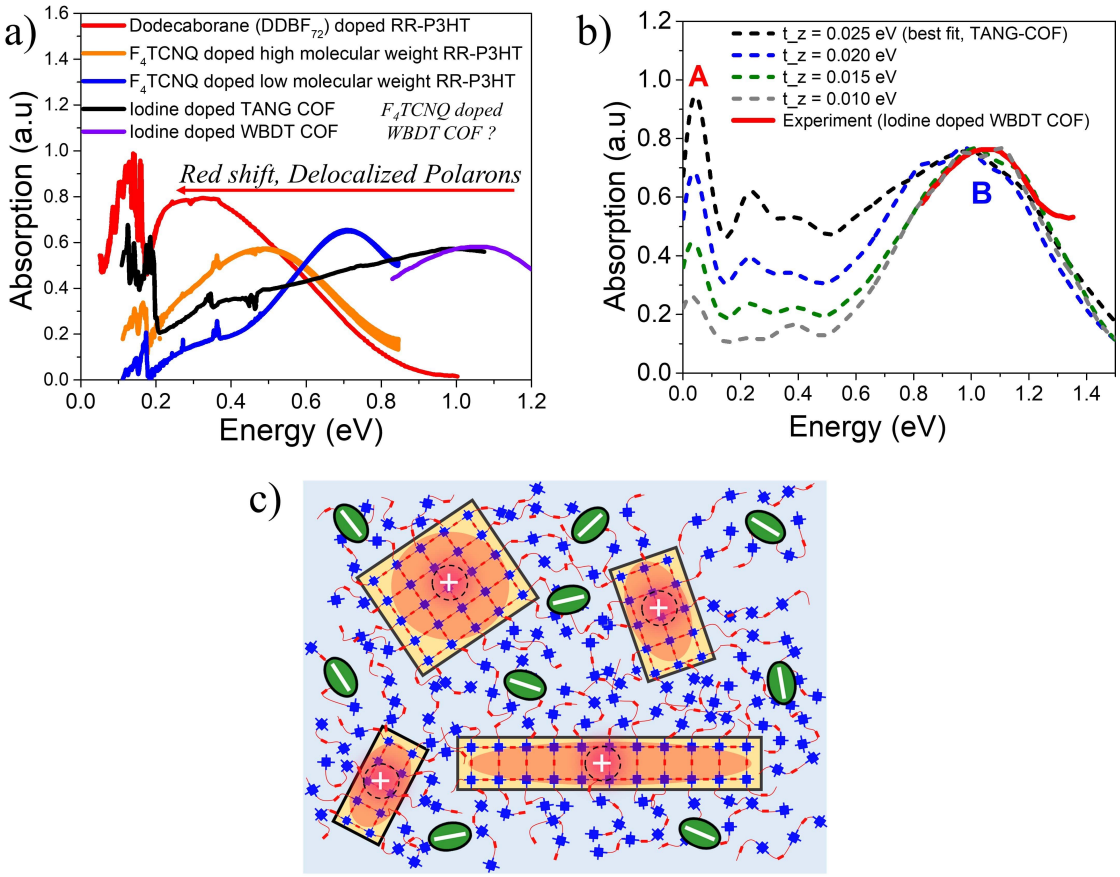

Figure 6: (a) Comparing the mid-IR absorption spectrum of doped polymers(replotted from Ref. 35, 53) and doped COFs (replotted from Ref. 31, 44) as a function of dopant type. (b) Comparison of the simulated IR spectrum (dashed) to the measured spectrum of iodine doped WBDT-COF.[44] (c) Sketch showing delocalized polarons within individual COF domains. Bulky F_4TCNQ dopants preferentially reside in the amorphous regions resulting in stable conductivity and crystalline frameworks.

the holes, which results in lower conductivity. While the peak B maximum for iodine doped WBDT COF appears at a similar position, the A/B peak ratio may or may not match. Here, we demonstrate that the A/B peak ratio in iodine doped COFs can be effectively used to monitor the extent of charge transport between the 2D layers.

Interlayer electronic coupling ($t_{inter-z}$) depends on several factors, including the monomer structure and planarity,[75–77] crystallinity,[78–81] nature of stacking (cofacial vs slipped),[82–84] and hydrogen bonding.[24,85–88] Using the same parameters that was used to reproduce the mid-IR absorption spectra of TANG COF, in the following analysis, we gradually increase

the CT integral along the z direction ($t_{inter-z}$). As shown in Fig. 6b, a gradual increase of the inter-framework coupling results in an increase of only the inter-framework component (peak A) of the absorption spectrum while leaving the intra-frameork component (peak B) relatively unchanged. Therefore, in the case of iodine doped COF films, a small A/B ratio in the infrared spectrum would imply that the hole movement is restricted within the 2D COF plane while a 3D delocalized polaron would yield a larger A/B ratio.

Interestingly, when doped with F_4TCNQ, no such peak appears at 1 eV and the spectrum measured in Ref. 44 is essentially flat in that energy range. F_4TCNQ doping results in higher conductivity which indicates greater delocalization of the polarons within the frameworks. Since an increase in polaron delocalization would result in a red shift of peak B, we predict the position of the peak B maximum to be somewhere below 0.75 eV. Another very interesting conclusion regarding the long-term crystallinity and stable conductivity of F_4TCNQ doped WBDT-COF can be drawn from the analysis of the interplay between pore-size and bulkiness of the dopant. F_4TCNQ, being a bulkier dopant compared to iodine, may not readily move into the WBDT-COF pores and may preferentially reside in the amorphous regions between crystalline domains or at the grain boundaries as illustrated in Fig. 6c, thus preserving the crystallinity of the frameworks and maintaining long-term stable conductivity. In the context of conjugated polymers, a recent study has shown that doping P3HT with an even bulkier dodecaborane (DDB-F_{72}) dopant yields higher hole mobility compared to when doped with F_4TCNQ.[35] The difference was attributed to a significant reduction in the electrostatic interactions between the hole and the bulky DDB-F_{72} counteranions that remain far away from the polymer backbone (2 nm) compared to F_4TCNQ counteranions (0.8 nm -1 nm). This increase in mobility and conductivity in DDB-F_{72}-doped P3HT is directly associated with increased polaron delocalization lengths, and displays a redshifted peak B and a much higher A/B ratio compared to when P3HT is doped with F_4TCNQ (see Fig. 6a). Similar conclusions were reached from the systematic analysis of the effects of counteranion size on polaron delocalization and mid-IR spectral signatures reported in Ref. 59. Therefore,

investigating the mid to near IR spectral signatures as a function of pore sizes, linker lengths, building blocks, and type of dopants will provide a critical understanding of the extent of intra- and inter-framework polaron transport, structure property relationships, effect of topology, and electrical properties of COF films.

Tetrathiafulvalene-based COFs

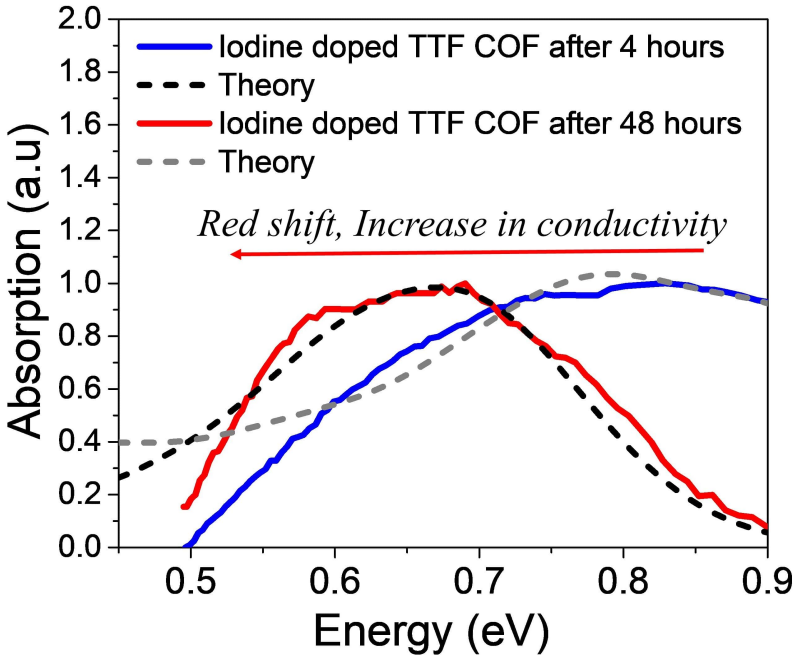

Figure 7: Comparison of the simulated IR spectrum (dashed) to the measured spectrum of iodine doped TTF-COFs at two different time intervals. Replotted and normalized from Ref. 41.

Finally, we discuss the IR spectral signatures of iodine and TCNQ doped TTF-COF films.[41] While TCNQ is unable to generate sufficient free charge carriers and, therefore, yields lower values of conductivity, iodine doped TTF-COF exhibits significantly greater conductivity. Time-dependent IR measurements carried out on iodine-doped TTF-COFs show evident spectral changes as a function of conductivity. As the conductivity increases, peak B redshifts to 0.6 eV and blue shifts back to 0.9 eV with a decrease in conductivity. The gradual increase in the spectral intensity upon iodine doping in the measured spectrum

reported in Ref. 41 arises from the generation of more free carriers. However, the red shift of the measured absorption spectrum at ∼0.6 eV (peak B) is indicative of the excess dopant anions residing relatively far away from the holes in the COF layers. Upon prolonged exposure to iodine, as the counteranions fill up all the trap/defect sites, further increase in dopant concentration results in more delocalized polarons since these new dopants most probably occupy the remaining vacant spaces available in the center of the pore or at the grain boundaries, far away from the framework backbone. As described in the previous sections, the relative position of the peak B maximum directly tracks the hole-counteranion distance. Using the same parameters that was used in the analysis of the spectrum measured for TANG-COF, we show that increasing the counteranion distance, from 0.40 nm to 0.50 nm, accurately captures the red-shift in the absorption spectrum. In our analysis of the spectrum of TTF-COF, we have only focused on the relative change in the position of the peak B maximum since the intensity of the measured spectrum reported in Ref. 41 was normalized to 1. Moreover, it is not possible to analyze the lineshape broadening since we do not have the full spectrum at our disposal, i.e how the spectrum unfolds at lower energies and what is the ratio of A/B. However, the time-dependent spectral broadening in the measured spectrum from Ref. 41 clearly suggests that increasing dopant concentrations results in an increased disorder within the frameworks. Interestingly, it should be noted that TTF-Phenyl-COF, which is characterized by longer linkers and larger pores (2.5 nm) compared to TTF-pyrene-COF (1.6 nm), indeed exhibits higher conductivity on iodine doping.[42] We hypothesize that smaller pore sizes would lead to stronger electrostatic interactions due to closer proximity and high density of the iodine dopants present inside the pores, thus resulting in trapped polarons and lower conductivity. However, smaller pores may be ideal if bulky dopants are used and might significantly improve device performance. While the increase (decrease) in conductivity is directly reflected in a red (blue) shift of the absorption spectra of TTF-COFs, some caution should be used in assuming that this is a universal signature. This trend may not hold if inter-domain charge transport is achieved in COFs since the electrical properties

entirely depend on long-range order and mesoscale connectivity between domains.[28,59]

It should be mentioned that in all our comparisons with the available experimental data, we have considered 3D tetragonal lattices. COF topologies vary across different structures. For example, 2D TANG COF is a superposition of kagome and honeycomb lattices while WBDT COF exhibits a dual pore kagome structure. Investigating the impact of topology on charge transport is beyond the scope of this current study and will be addressed in future. However, the general conclusions for doped COFs will remain unchanged. As shown in Fig. 5b, our comparison with the measured spectrum involves the configuration where the presence of the anion greatly localizes the polaron wavefunction to roughly one unit along the x and z axes. This small subspace is inherently present in all topologies as shown schematically in the Supporting Information (Fig. S5). The effects of topology may become more prominent in the case of unbound holes which, being free to delocalize over the entire framework, can take advantage of the 3D topological arrangement. In such scenarios, the spectrum may slightly vary and the inter- and intra-framework components will be different. Additional experiments and simulations are needed to completely characterize the impact of topology on charge migration in 2D-COFs.[89]

Conclusion and Outlook

To summarize, we have provided a comprehensive and detailed understanding of the microscopic structure-property relationships and charge transport physics of 2D COFs. A robust theoretical model was developed which quantitatively describes the IR line shape for chemically induced polarons in COFs and explains the origin of the two main bands in the absorption spectrum. Based on our discussions, we have shown that the low energy spectral signatures, in particular, the position of peak B and the A/B peak ratio can be effectively used to extract fundamental information about the disorder induced local structural arrangement within the frameworks, location of the dopant counteranions in the COF matrix,

and the extent of intra- and interframework polaron delocalization. Spectral signatures are identified which attributes lower conductivity in doped COFs to strong coulomb binding and the presence of high defect density within the frameworks. In order to address these shortcomings and improve conductivity in 2D COFs, well known requirements such as extended π-conjugation, high degree of crystallinity, long range ordered domains, and efficient overlap of the electronic wavefunctions between the 2D-layers need to be met. However, in the case doped COF films, key new research directions would involve an in-depth analysis of the mid-IR spectral changes as a function of linker lengths, type of linkers, pore sizes, topology, type of dopants, and dopant concentrations. Time dependant as well as dopant concentration dependant FTIR measurements of doped COF films will provide a better understanding of the dopant-hole interactions, morphologies, and the complex disordered landscape of various COF structures. While iodine doping have resulted in increased conductivities by several orders of magnitude, the conductivities are unstable and reversible. Therefore, in order to achieve permanent, stable and meaningful increase in conductivity for potential device applications, dopants which do not infiltrate the frameworks and maximize localization effects are crucial. Bulky p-dopants (F_4TCNQ, DDB-F_{72}) and dopants having high electron affinity[58,90] can be used in conjunction with electroactive building blocks to improve final device performance. The importance of electroactive building blocks was pointed out in Ref. 44 where the authors showed that using benzodithiophene as a linker resulted in more efficient doping compared to terephthalaldehyde.

In the absence of chemical dopants, "free" holes can be generated either by photoinduced absorption spectroscopy or charge modulation spectroscopy (CMS).[25,28,33,56,71] Creation of free holes generally yields higher mobility since their movement is not restricted by dopant counteranions. Low energy polaron signals have been used to characterize the local structural order, chain alignment, morphology and crystallinity of conjuagted polymers in the vicinity of the charge carriers.[27,71] CMS measurements on high molecular weight 100% RR-P3HT showed much higher charge carrier mobilities and a A/B peak ratio of ≈ 1.7.[28] An

even higher A/B ratio (≈ 2.0) was reported in photoinduced IR spectra of donor–acceptor polymer PCPDTBT blends with electron acceptor PCBM, although the mobilities were not reported.[27] CM measurements on various COF structures can reveal critical insights into the structure-property relationships and factors affecting hole movement in the frameworks.

While unpolarized mid-IR measurements are crucial, polarized measurements on oriented COF films can be a significant step forward in advancing our fundamental understanding of polaron phoptophysics and transport signatures of 2D COFs. To unambiguously understand the anisotropic nature of hole coherence in doped COF films, more experiments need to be conducted on aligned (doped and undoped) COF samples. From a theoretical standpoint, important future directions would be focused on investigating the effect of topology on the charge transport and the effect of various dopants on the electronic band structure of prototypical COF structures. We hope that our detailed theoretical investigation and a mini-perspective will not only bridge the gap between the COFs and polymer communities but also motivate future exciting experiments along the same lines which might pave the way for better COF/polymer-based devices for a wide range of optoelectronics applications.

Acknowledgement

This research was supported by the National Science Foundation through grant No. 1704063. This research used resources of the National Energy Research Scientific Computing Center (NERSC), which is supported by the Office of Science of the U.S. Department of Energy under Contract DE- AC02-05CH11231, as well as the Triton Shared Computing Cluster (TSCC) at the San Diego Supercomputer Center (SDSC). The softwares PETSc and SLEPc were used to diagonalize the Hamiltonian.[91–93]

Supporting Information Available

The 3D Holstein Hamiltonian for tetragonal COF structures is given. The expressions for

IR absorption spectrum and coherence function along with a brief explanation of the fundamental nature and origin of the two bands A and B are discussed. Parameters used to define the Hamiltonian for the figures in the main text are provided.

References

(1) Cote, A. P.; Benin, A. I.; Ockwig, N. W.; O'Keeffe, M.; Matzger, A. J.; Yaghi, O. M. Porous, crystalline, covalent organic frameworks. *Science* **2005**, *310*, 1166–1170.

(2) Uribe-Romo, F. J.; Hunt, J. R.; Furukawa, H.; Klock, C.; O'Keeffe, M.; Yaghi, O. M. A crystalline imine-linked 3-D porous covalent organic framework. *J. Am. Chem. Soc.* **2009**, *131*, 4570–4571.

(3) Uribe-Romo, F. J.; Doonan, C. J.; Furukawa, H.; Oisaki, K.; Yaghi, O. M. Crystalline covalent organic frameworks with hydrazone linkages. *J. Am. Chem. Soc.* **2011**, *133*, 11478–11481.

(4) Kandambeth, S.; Dey, K.; Banerjee, R. Covalent organic frameworks: chemistry beyond the structure. *J. Am. Chem. Soc.* **2018**, *141*, 1807–1822.

(5) Dey, K.; Bhunia, S.; Sasmal, H. S.; Reddy, C. M.; Banerjee, R. Self-Assembly-Driven Nanomechanics in Porous Covalent Organic Framework Thin Films. *J. Am. Chem. Soc.*

(6) Segura, J. L.; Mancheño, M. J.; Zamora, F. Covalent organic frameworks based on Schiff-base chemistry: synthesis, properties and potential applications. *Chem. Soc. Rev.* **2016**, *45*, 5635–5671.

(7) Lohse, M. S.; Bein, T. Covalent organic frameworks: structures, synthesis, and applications. *Adv. Funct. Mater.* **2018**, *28*, 1705553.

(8) Xu, L.; Ding, S.-Y.; Liu, J.; Sun, J.; Wang, W.; Zheng, Q.-Y. Highly crystalline covalent organic frameworks from flexible building blocks. *ChemComm* **2016**, *52*, 4706–4709.

(9) El-Kaderi, H. M.; Hunt, J. R.; Mendoza-Cortés, J. L.; Côté, A. P.; Taylor, R. E.; O'Keeffe, M.; Yaghi, O. M. Designed synthesis of 3D covalent organic frameworks. *Science* **2007**, *316*, 268–272.

(10) Furukawa, H.; Yaghi, O. M. Storage of hydrogen, methane, and carbon dioxide in highly porous covalent organic frameworks for clean energy applications. *J. Am. Chem. Soc.* **2009**, *131*, 8875–8883.

(11) Jin, E.; Asada, M.; Xu, Q.; Dalapati, S.; Addicoat, M. A.; Brady, M. A.; Xu, H.; Nakamura, T.; Heine, T.; Chen, Q., et al. Two-dimensional sp2 carbon–conjugated covalent organic frameworks. *Science* **2017**, *357*, 673–676.

(12) Bertrand, G. H.; Michaelis, V. K.; Ong, T.-C.; Griffin, R. G.; Dincă, M. Thiophene-based covalent organic frameworks. *Proc. Natl. Acad. Sci.* **2013**, *110*, 4923–4928.

(13) Colson, J. W.; Woll, A. R.; Mukherjee, A.; Levendorf, M. P.; Spitler, E. L.; Shields, V. B.; Spencer, M. G.; Park, J.; Dichtel, W. R. Oriented 2D covalent organic framework thin films on single-layer graphene. *Science* **2011**, *332*, 228–231.

(14) Evans, A. M.; Parent, L. R.; Flanders, N. C.; Bisbey, R. P.; Vitaku, E.; Kirschner, M. S.; Schaller, R. D.; Chen, L. X.; Gianneschi, N. C.; Dichtel, W. R. Seeded growth of single-crystal two-dimensional covalent organic frameworks. *Science* **2018**, *361*, 52–57.

(15) Flanders, N. C.; Kirschner, M. S.; Kim, P.; Fauvell, T. J.; Evans, A. M.; Helweh, W.; Spencer, A. P.; Schaller, R. D.; Dichtel, W. R.; Chen, L. X. Large Exciton Diffusion Coefficients in Two-Dimensional Covalent Organic Frameworks with Different Domain Sizes Revealed by Ultrafast Exciton Dynamics. *J. Am. Chem. Soc.* **2020**,

(16) Chen, X.; Addicoat, M.; Irle, S.; Nagai, A.; Jiang, D. Control of crystallinity and porosity of covalent organic frameworks by managing interlayer interactions based on self-complementary π-electronic force. *J. Am. Chem. Soc.* **2013**, *135*, 546–549.

(17) Haug, W. K.; Moscarello, E. M.; Wolfson, E. R.; McGrier, P. L. The luminescent and photophysical properties of covalent organic frameworks. *Chem. Soc. Rev.* **2020**, *49*, 839–864.

(18) Jakowetz, A. C.; Hinrichsen, T. F.; Ascherl, L.; Sick, T.; Calik, M.; Auras, F.; Medina, D. D.; Friend, R. H.; Rao, A.; Bein, T. Excited-State Dynamics in Fully Conjugated 2D Covalent Organic Frameworks. *J. Am. Chem. Soc.* **2019**, *141*, 11565–11571.

(19) Ascherl, L.; Evans, E. W.; Gorman, J.; Orsborne, S.; Bessinger, D.; Bein, T.; Friend, R. H.; Auras, F. Perylene-Based Covalent Organic Frameworks for Acid Vapor Sensing. *J. Am. Chem. Soc.* **2019**, *141*, 15693–15699.

(20) Li, R. L.; Flanders, N. C.; Evans, A. M.; Ji, W.; Castano, I.; Chen, L. X.; Gianneschi, N. C.; Dichtel, W. R. Controlled growth of imine-linked two-dimensional covalent organic framework nanoparticles. *Chem. Sci.* **2019**, *10*, 3796–3801.

(21) Burke, D. W.; Sun, C.; Castano, I.; Flanders, N. C.; Evans, A. M.; Vitaku, E.; McLeod, D. C.; Lambeth, R. H.; Chen, L. X.; Gianneschi, N. C., et al. Acid Exfoliation of Imine-linked Covalent Organic Frameworks Enables Solution Processing into Crystalline Thin Films. *Angew. Chem. Int. Ed.* **2020**, *59*, 5165–5171.

(22) Liu, R.; Tan, K. T.; Gong, Y.; Chen, Y.; Li, Z.; Xie, S.; He, T.; Lu, Z.; Yang, H.; Jiang, D. Covalent organic frameworks: an ideal platform for designing ordered materials and advanced applications. *Chem. Soc. Rev.* **2021**,

(23) Kang, C.; Zhang, Z.; Wee, V.; Usadi, A. K.; Calabro, D. C.; Baugh, L. S.; Wang, S.; Wang, Y.; Zhao, D. Interlayer Shifting in Two-Dimensional Covalent Organic Frameworks. *J. Am. Chem. Soc.* **2020**, *142*, 12995–13002.

(24) Li, X.; Qiao, J.; Chee, S. W.; Xu, H.-S.; Zhao, X.; Choi, H. S.; Yu, W.; Quek, S. Y.; Mirsaidov, U.; Loh, K. P. Rapid, Scalable Construction of Highly Crystalline Acylhydra-

zone Two-dimensional Covalent Organic Frameworks via Dipole-Induced Antiparallel Stacking. *J. Am. Chem. Soc.* **2020**, *142*, 4932–4943.

(25) Sirringhaus, H.; Brown, P.; Friend, R.; Nielsen, M. M.; Bechgaard, K.; Langeveld-Voss, B.; Spiering, A.; Janssen, R. A.; Meijer, E.; Herwig, P., et al. Two-dimensional charge transport in self-organized, high-mobility conjugated polymers. *Nature* **1999**, *401*, 685–688.

(26) Österbacka, R.; An, C. P.; Jiang, X.; Vardeny, Z. V. Two-dimensional electronic excitations in self-assembled conjugated polymer nanocrystals. *Science* **2000**, *287*, 839–842.

(27) Kahmann, S.; Loi, M. A.; Brabec, C. J. Delocalisation softens polaron electronic transitions and vibrational modes in conjugated polymers. *J. Mater. Chem. C* **2018**, *6*, 6008–6013.

(28) Chew, A. R.; Ghosh, R.; Pakhnyuk, V.; Onorato, J.; Davidson, E. C.; Segalman, R. A.; Luscombe, C. K.; Spano, F. C.; Salleo, A. Unraveling the effect of conformational and electronic disorder in the charge transport processes of semiconducting polymers. *Adv. Funct. Mater.* **2018**, *28*, 1804142.

(29) Ghosh, R.; Spano, F. C. Excitons and Polarons in Organic Materials. *Acc. Chem. Res.* **2020**, *53*, 2201–2211.

(30) Voss, M. G.; Scholes, D. T.; Challa, J. R.; Schwartz, B. J. Ultrafast transient absorption spectroscopy of doped P3HT films: distinguishing free and trapped polarons. *Faraday Discuss.* **2019**, *216*, 339–362.

(31) Lakshmi, V.; Liu, C.-H.; Rajeswara Rao, M.; Chen, Y.; Fang, Y.; Dadvand, A.; Hamzehpoor, E.; Sakai-Otsuka, Y.; Stein, R. S.; Perepichka, D. F. A Two-Dimensional Poly (azatriangulene) Covalent Organic Framework with Semiconducting and Paramagnetic States. *J. Am. Chem. Soc.* **2020**, *142*, 2155–2160.

(32) Jiang, X. M.; Österbacka, R.; Korovyanko, O.; An, C. P.; Horovitz, B.; Janssen, R. A.; Vardeny, Z. V. Spectroscopic studies of photoexcitations in regioregular and regiorandom polythiophene films. *Adv. Funct. Mater.* **2002**, *12*, 587–597.

(33) Chang, J.-F.; Clark, J.; Zhao, N.; Sirringhaus, H.; Breiby, D. W.; Andreasen, J. W.; Nielsen, M. M.; Giles, M.; Heeney, M.; McCulloch, I. Molecular-weight dependence of interchain polaron delocalization and exciton bandwidth in high-mobility conjugated polymers. *Phys. Rev. B* **2006**, *74*, 115318.

(34) Brown, P. J.; Thomas, D. S.; Köhler, A.; Wilson, J. S.; Kim, J.-S.; Ramsdale, C. M.; Sirringhaus, H.; Friend, R. H. Effect of interchain interactions on the absorption and emission of poly (3-hexylthiophene). *Phys. Rev. B* **2003**, *67*, 064203.

(35) Aubry, T. J.; Axtell, J. C.; Basile, V. M.; Winchell, K.; Lindemuth, J. R.; Porter, T. M.; Liu, J.-Y.; Alexandrova, A. N.; Kubiak, C. P.; Tolbert, S. H., et al. Dodecaborane-Based Dopants Designed to Shield Anion Electrostatics Lead to Increased Carrier Mobility in a Doped Conjugated Polymer. *Adv. Mater.* **2019**, *31*, 1805647.

(36) Enengl, C.; Enengl, S.; Pluczyk, S.; Havlicek, M.; Lapkowski, M.; Neugebauer, H.; Ehrenfreund, E. Doping-Induced Absorption Bands in P3HT: Polarons and Bipolarons. *Chemphyschem* **2016**, *17*, 3836–3844.

(37) Yu, H.; Wang, D. Metal-free magnetism in chemically doped covalent organic frameworks. *J. Am. Chem. Soc.* **2020**, *142*, 11013–11021.

(38) Meng, Z.; Stolz, R. M.; Mirica, K. A. Two-dimensional chemiresistive covalent organic framework with high intrinsic conductivity. *J. Am. Chem. Soc.* **2019**, *141*, 11929–11937.

(39) Wang, C.; Wang, Y.; Ge, R.; Song, X.; Xing, X.; Jiang, Q.; Lu, H.; Hao, C.; Guo, X.; Gao, Y., et al. A 3D covalent organic framework with exceptionally high iodine capture capability. *Chem. Eur. J.* **2018**, *24*, 585–589.

(40) Wang, L.; Dong, B.; Ge, R.; Jiang, F.; Xu, J. Fluorene-based two-dimensional covalent organic framework with thermoelectric properties through doping. *ACS Appl. Mater. Interfaces* **2017**, *9*, 7108–7114.

(41) Cai, S.-L.; Zhang, Y.-B.; Pun, A. B.; He, B.; Yang, J.; Toma, F. M.; Sharp, I. D.; Yaghi, O. M.; Fan, J.; Zheng, S.-R., et al. Tunable electrical conductivity in oriented thin films of tetrathiafulvalene-based covalent organic framework. *Chem. Sci.* **2014**, *5*, 4693–4700.

(42) Jin, S.; Sakurai, T.; Kowalczyk, T.; Dalapati, S.; Xu, F.; Wei, H.; Chen, X.; Gao, J.; Seki, S.; Irle, S., et al. Two-dimensional tetrathiafulvalene covalent organic frameworks: towards latticed conductive organic salts. *Chem. Eur. J.* **2014**, *20*, 14608–14613.

(43) Li, H.; Chang, J.; Li, S.; Guan, X.; Li, D.; Li, C.; Tang, L.; Xue, M.; Yan, Y.; Valtchev, V., et al. Three-dimensional tetrathiafulvalene-based covalent organic frameworks for tunable electrical conductivity. *J. Am. Chem. Soc.* **2019**, *141*, 13324–13329.

(44) Rotter, J. M.; Guntermann, R.; Auth, M.; Mähringer, A.; Sperlich, A.; Dyakonov, V.; Medina, D. D.; Bein, T. Highly conducting Wurster-type twisted covalent organic frameworks. *Chem. Sci.* **2020**, *11*, 12843–12853.

(45) Medina, D. D.; Petrus, M. L.; Jumabekov, A. N.; Margraf, J. T.; Weinberger, S.; Rotter, J. M.; Clark, T.; Bein, T. Directional charge-carrier transport in oriented benzodithiophene covalent organic framework thin films. *ACS Nano* **2017**, *11*, 2706–2713.

(46) Qi, H.; Sahabudeen, H.; Liang, B.; Položij, M.; Addicoat, M. A.; Gorelik, T. E.; Hambsch, M.; Mundszinger, M.; Park, S.; Lotsch, B. V., et al. Near–atomic-scale observation of grain boundaries in a layer-stacked two-dimensional polymer. *Sci. Adv.* **2020**, *6*, eabb5976.

(47) Castano, I.; Evans, A. M.; Reis, R. d.; Dravid, V. P.; Gianneschi, N. C.; Dichtel, W. R.

Mapping Grains, Boundaries, and Defects in 2D Covalent Organic Framework Thin Films. *Chem. Mater.* **2021**,

(48) Luo, M.; Yang, Q.; Yang, W.; Wang, J.; He, F.; Liu, K.; Cao, H.; Yan, H. Defects engineering leads to enhanced photocatalytic H2 evolution on graphitic carbon nitride–covalent organic framework nanosheet composite. *Small* **2020**, *16*, 2001100.

(49) Pütz, A. M.; Terban, M. W.; Bette, S.; Haase, F.; Dinnebier, R. E.; Lotsch, B. V. Total scattering reveals the hidden stacking disorder in a 2D covalent organic framework. *Chem. Sci.* **2020**,

(50) Nguyen, V.; Grünwald, M. Microscopic origins of poor crystallinity in the synthesis of covalent organic framework COF-5. *J. Am. Chem. Soc.* **2018**, *140*, 3306–3311.

(51) Tanaka, H.; Wakamatsu, A.; Kondo, M.; Kawamura, S.; Kuroda, S.-i.; Shimoi, Y.; Park, W.-T.; Noh, Y.-Y.; Takenobu, T. Microscopic observation of efficient charge transport processes across domain boundaries in donor-acceptor-type conjugated polymers. *Commun. Phys.* **2019**, *2*, 1–10.

(52) Ghosh, R.; Pochas, C. M.; Spano, F. C. Polaron delocalization in conjugated polymer films. *J. Phys. Chem. C* **2016**, *120*, 11394–11406.

(53) Ghosh, R.; Chew, A. R.; Onorato, J.; Pakhnyuk, V.; Luscombe, C. K.; Salleo, A.; Spano, F. C. Spectral signatures and spatial coherence of bound and unbound polarons in p3ht films: Theory versus experiment. *J. Phys. Chem. C* **2018**, *122*, 18048–18060.

(54) Ghosh, R.; Luscombe, C. K.; Hambsch, M.; Mannsfeld, S. C.; Salleo, A.; Spano, F. C. Anisotropic polaron delocalization in conjugated homopolymers and donor–acceptor copolymers. *Chem. Mater.* **2019**, *31*, 7033–7045.

(55) Scholes, D. T.; Yee, P. Y.; Lindemuth, J. R.; Kang, H.; Onorato, J.; Ghosh, R.; Luscombe, C. K.; Spano, F. C.; Tolbert, S. H.; Schwartz, B. J. The Effects of Crystallinity

on Charge Transport and the Structure of Sequentially Processed F4TCNQ-Doped Conjugated Polymer Films. *Adv. Funct. Mater.* **2017**, *27*, 1702654.

(56) Chew, A. R.; Ghosh, R.; Shang, Z.; Spano, F. C.; Salleo, A. Sequential doping reveals the importance of amorphous chain rigidity in charge transport of semi-crystalline polymers. *J. Phys. Chem. Lett.* **2017**, *8*, 4974–4980.

(57) Finn, P. A.; Jacobs, I. E.; Armitage, J.; Wu, R.; Paulsen, B. D.; Freeley, M.; Palma, M.; Rivnay, J.; Sirringhaus, H.; Nielsen, C. B. Effect of polar side chains on neutral and p-doped polythiophene. *J. Mater. Chem. C* **2020**, *8*, 16216–16223.

(58) Aubry, T. J.; Winchell, K.; Salamat, C. Z.; Basile, V. M.; Lindemuth, J. R.; Stauber, J. M.; Axtell, J. C.; Kubena, R. M.; Phan, M. D.; Bird, M. J., et al. Tunable Dopants with Intrinsic Counterion Separation Reveal the Effects of Electron Affinity on Dopant Intercalation and Free Carrier Production in Sequentially Doped Conjugated Polymer Films. *Adv. Funct. Mater.* **2020**, 2001800.

(59) Thomas, E. M.; Peterson, K. A.; Balzer, A. H.; Rawlings, D.; Stingelin, N.; Segalman, R. A.; Chabinyc, M. L. Effects of Counter-Ion Size on Delocalization of Carriers and Stability of Doped Semiconducting Polymers. *Adv. Electron. Mater.* **2020**, *6*, 2000595.

(60) Pochas, C. M.; Spano, F. C. New insights on the nature of two-dimensional polarons in semiconducting polymers: Infrared absorption in poly (3-hexylthiophene). *J. Chem. Phys.* **2014**, *140*, 244902.

(61) Hofmann, A. I.; Kroon, R.; Zokaei, S.; Järsvall, E.; Malacrida, C.; Ludwigs, S.; Biskup, T.; Müller, C. Chemical Doping of Conjugated Polymers with the Strong Oxidant Magic Blue. *Adv. Electron. Mater.* 2000249.

(62) Haase, F.; Lotsch, B. V. Solving the COF trilemma: towards crystalline, stable and functional covalent organic frameworks. *Chem. Soc. Rev.* **2020**, *49*, 8469–8500.

(63) Auras, F.; Ascherl, L.; Hakimioun, A. H.; Margraf, J. T.; Hanusch, F. C.; Reuter, S.; Bessinger, D.; Döblinger, M.; Hettstedt, C.; Karaghiosoff, K., et al. Synchronized offset stacking: a concept for growing large-domain and highly crystalline 2D covalent organic frameworks. *J. Am. Chem. Soc.* **2016**, *138*, 16703–16710.

(64) Martínez-Abadía, M.; Mateo-Alonso, A. Structural Approaches to Control Interlayer Interactions in 2D Covalent Organic Frameworks. *Adv. Mater.* **2020**, *32*, 2002366.

(65) Hestand, N. J.; Spano, F. C. Interference between Coulombic and CT-mediated couplings in molecular aggregates: H-to J-aggregate transformation in perylene-based π-stacks. *J. Chem. Phys.* **2015**, *143*, 244707.

(66) Hestand, N. J.; Spano, F. C. Molecular aggregate photophysics beyond the Kasha model: novel design principles for organic materials. *Acc. Chem. Res.* **2017**, *50*, 341–350.

(67) Hestand, N. J.; Spano, F. C. Expanded theory of H-and J-molecular aggregates: the effects of vibronic coupling and intermolecular charge transfer. *Chem. Rev.* **2018**, *118*, 7069–7163.

(68) Spano, F. C. The spectral signatures of Frenkel polarons in H-and J-aggregates. *Acc. Chem. Res.* **2010**, *43*, 429–439.

(69) Spano, F. C. Excitons in conjugated oligomer aggregates, films, and crystals. *Annu. Rev. Phys. Chem.* **2006**, *57*, 217–243.

(70) Thomas, S.; Li, H.; Dasari, R. R.; Evans, A. M.; Castano, I.; Allen, T. G.; Reid, O. G.; Rumbles, G.; Dichtel, W. R.; Gianneschi, N. C., et al. Design and synthesis of two-dimensional covalent organic frameworks with four-arm cores: prediction of remarkable ambipolar charge-transport properties. *Mater. Horizons* **2019**, *6*, 1868–1876.

(71) Kahmann, S.; Fazzi, D.; Matt, G. J.; Thiel, W.; Loi, M. A.; Brabec, C. J. Polarons in narrow band gap polymers probed over the entire infrared range: a joint experimental and theoretical investigation. *J. Phys. Chem. Lett.* **2016**, *7*, 4438–4444.

(72) Fratini, S.; Nikolka, M.; Salleo, A.; Schweicher, G.; Sirringhaus, H. Charge transport in high-mobility conjugated polymers and molecular semiconductors. *Nat. Mater.* **2020**, *19*, 491–502.

(73) Noriega, R.; Rivnay, J.; Vandewal, K.; Koch, F. P.; Stingelin, N.; Smith, P.; Toney, M. F.; Salleo, A. A general relationship between disorder, aggregation and charge transport in conjugated polymers. *Nat. Mater.* **2013**, *12*, 1038–1044.

(74) Gu, K.; Snyder, C. R.; Onorato, J.; Luscombe, C. K.; Bosse, A. W.; Loo, Y.-L. Assessing the huang–brown description of tie chains for charge transport in conjugated polymers. *ACS Macro Lett.* **2018**, *7*, 1333–1338.

(75) Vyas, V. S.; Haase, F.; Stegbauer, L.; Savasci, G.; Podjaski, F.; Ochsenfeld, C.; Lotsch, B. V. A tunable azine covalent organic framework platform for visible light-induced hydrogen generation. *Nat. Commun.* **2015**, *6*, 1–9.

(76) Haase, F.; Banerjee, T.; Savasci, G.; Ochsenfeld, C.; Lotsch, B. V. Structure–property–activity relationships in a pyridine containing azine-linked covalent organic framework for photocatalytic hydrogen evolution. *Faraday Discuss.* **2017**, *201*, 247–264.

(77) El-Mahdy, A. F.; Kuo, C.-H.; Alshehri, A.; Young, C.; Yamauchi, Y.; Kim, J.; Kuo, S.-W. Strategic design of triphenylamine-and triphenyltriazine-based two-dimensional covalent organic frameworks for CO 2 uptake and energy storage. *J. Mater. Chem. A*

(78) Tilford, R. W.; Mugavero III, S. J.; Pellechia, P. J.; Lavigne, J. J. Tailoring microporosity in covalent organic frameworks. *Adv. Mater.* **2008**, *20*, 2741–2746.

(79) Lanni, L. M.; Tilford, R. W.; Bharathy, M.; Lavigne, J. J. Enhanced hydrolytic stability of self-assembling alkylated two-dimensional covalent organic frameworks. *J. Am. Chem. Soc.* **2011**, *133*, 13975–13983.

(80) Thompson, C. M.; Occhialini, G.; McCandless, G. T.; Alahakoon, S. B.; Cameron, V.; Nielsen, S. O.; Smaldone, R. A. Computational and experimental studies on the effects of monomer planarity on covalent organic framework formation. *J. Am. Chem. Soc.* **2017**, *139*, 10506–10513.

(81) Keller, N.; Bessinger, D.; Reuter, S.; Calik, M.; Ascherl, L.; Hanusch, F. C.; Auras, F.; Bein, T. Oligothiophene-bridged conjugated covalent organic frameworks. *J. Am. Chem. Soc.* **2017**, *139*, 8194–8199.

(82) Yin, H.-Q.; Yin, F.; Yin, X.-B. Strong dual emission in covalent organic frameworks induced by ESIPT. *Chem. Sci.* **2019**, *10*, 11103–11109.

(83) Albacete, P.; Martinez, J. I.; Li, X.; Lopez-Moreno, A.; Mena-Hernando, S.; Platero-Prats, A. E.; Montoro, C.; Loh, K. P.; Perez, E. M.; Zamora, F. Layer-stacking-driven fluorescence in a two-dimensional imine-linked covalent organic framework. *J. Am. Chem. Soc.* **2018**, *140*, 12922–12929.

(84) Wu, X.; Han, X.; Liu, Y.; Liu, Y.; Cui, Y. Control interlayer stacking and chemical stability of two-dimensional covalent organic frameworks via steric tuning. *J. Am. Chem. Soc.* **2018**, *140*, 16124–16133.

(85) Halder, A.; Ghosh, M.; Khayum M, A.; Bera, S.; Addicoat, M.; Sasmal, H. S.; Karak, S.; Kurungot, S.; Banerjee, R. Interlayer hydrogen-bonded covalent organic frameworks as high-performance supercapacitors. *J. Am. Chem. Soc.* **2018**, *140*, 10941–10945.

(86) Halder, A.; Karak, S.; Addicoat, M.; Bera, S.; Chakraborty, A.; Kunjattu, S. H.; Pachfule, P.; Heine, T.; Banerjee, R. Ultrastable imine-based covalent organic frameworks

for sulfuric acid recovery: an effect of interlayer hydrogen bonding. *Angew. Chem. Int. Ed.* **2018**, *57*, 5797–5802.

(87) Li, X.; Gao, Q.; Wang, J.; Chen, Y.; Chen, Z.-H.; Xu, H.-S.; Tang, W.; Leng, K.; Ning, G.-H.; Wu, J., et al. Tuneable near white-emissive two-dimensional covalent organic frameworks. *Nat. Commun.* **2018**, *9*, 1–9.

(88) Alahakoon, S. B.; Tan, K.; Pandey, H.; Diwakara, S. D.; McCandless, G. T.; Grinffiel, D. I.; Durand-Silva, A.; Thonhauser, T.; Smaldone, R. A. 2D-Covalent Organic Frameworks with Interlayer Hydrogen Bonding Oriented through Designed Nonplanarity. *J. Am. Chem. Soc.* **2020**, *142*, 12987–12994.

(89) Jin, E.; Geng, K.; Lee, K. H.; Jiang, W.; Li, J.; Jiang, Q.; Irle, S.; Jiang, D. Topology-Templated Synthesis of Crystalline Porous Covalent Organic Frameworks. *Angew. Chem. Int. Ed.* **2020**, *132*, 12260–12267.

(90) Saska, J.; Gonel, G.; Bedolla-Valdez, Z. I.; Aronow, S. D.; Shevchenko, N. E.; Dudnik, A. S.; Moulé, A. J.; Mascal, M. A Freely Soluble, High Electron Affinity Molecular Dopant for Solution Processing of Organic Semiconductors. *Chem. Mater.* **2019**, *31*, 1500–1506.

(91) Hernandez, V.; Roman, J. E.; Vidal, V. SLEPc: A scalable and flexible toolkit for the solution of eigenvalue problems. *ACM Trans. Math. Software* **2005**, *31*, 351–362.

(92) Roman, J. E.; Campos, C.; Romero, E.; Tomas, A. *SLEPc Users Manual*; 2020.

(93) Balay, S. et al. PETSc Web page. `https://www.mcs.anl.gov/petsc`, 2019; `https://www.mcs.anl.gov/petsc`.